PCCP

Physical Chemistry Chemical Physics

www.rsc.org/pccp

Volume 13 | Number 45 | 7 December 2011 | Pages 20023–20482

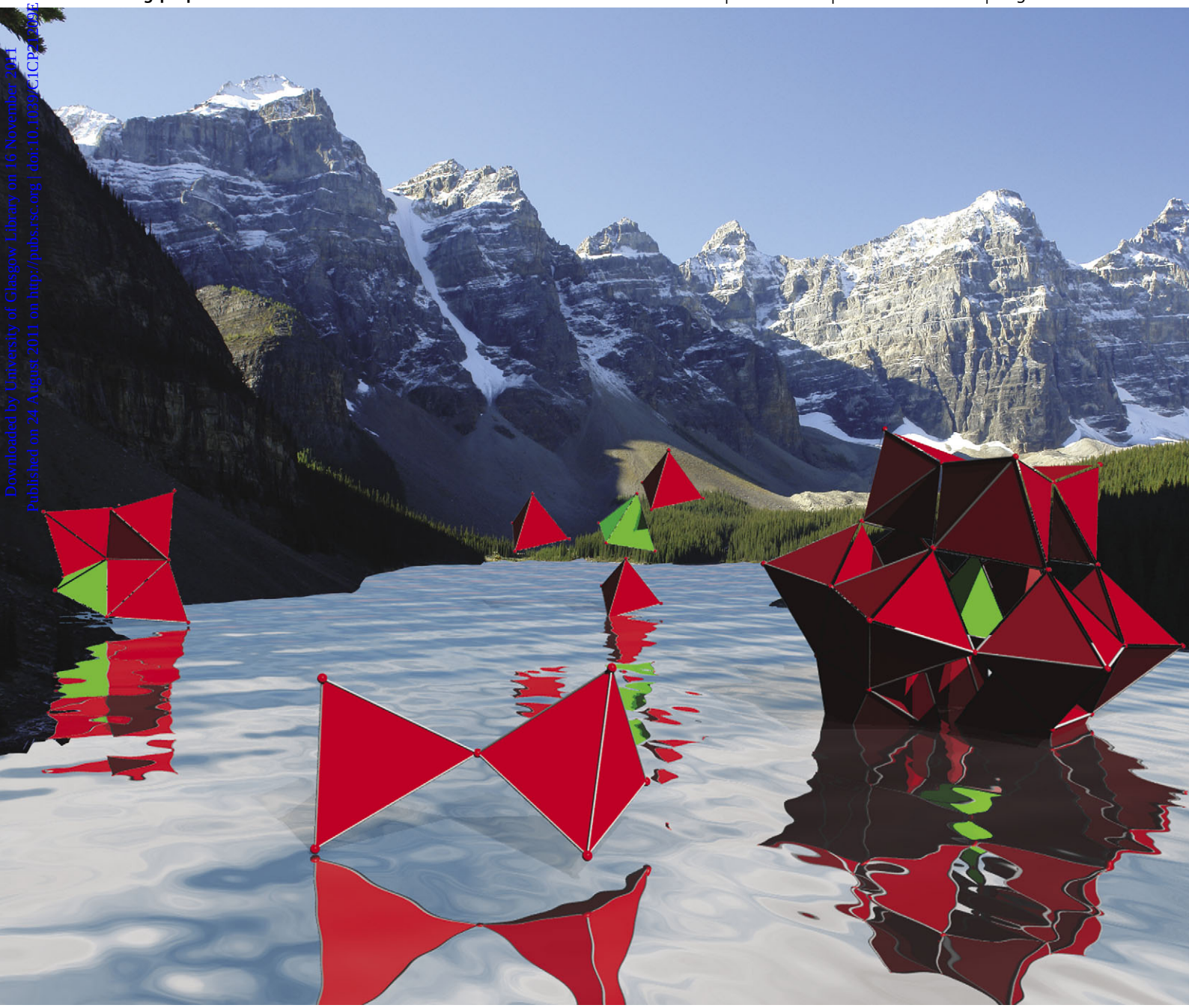

ISSN 1463-9076

1463-9076(2011)13:45;1-P

PCCP

Dynamic Article Links
View Online

Cite this: *Phys. Chem. Chem. Phys.*, 2011, **13**, 20136–20145

www.rsc.org/pccp

PAPER

Connecting theory with experiment to understand the initial nucleation steps of heteropolyoxometalate clusters†

Laia Vilà-Nadal,[a] Scott G. Mitchell,[b] Antonio Rodríguez-Fortea,*[a] Haralampos N. Miras,[b] Leroy Cronin*[b] and Josep M. Poblet*[a]

Received 16th April 2011, Accepted 26th July 2011
DOI: 10.1039/c1cp21209e

A complimentary combination of Density Functional Theory (DFT) methodology and Electrospray Ionization-Mass Spectrometry (ESI-MS) has been utilized to increase our limited understanding of the first nucleation steps in the formation of the $[XM_{12}O_{40}]^{n-}$ Keggin polyoxometalates (POMs) (where addenda metal atom M = W or Mo, and the heteroatom X = P or As). We postulate that the first key steps of nucleation into discrete, high nuclearity heteropolyanions proceed *via* the formation of isodinuclear species (*e.g.* $[M_2O_7]^{2-}$), which undergo successive steps of protonation and water condensation to form a heterotrinuclear fragment, which acts as a template for the constituent parts required for subsequent aggregation and formation of the plenary Keggin heteropolyanion. The stability of calculated structures of the numerous postulated intermediates has been analysed and discussed in detail, and these results complemented using experimental mass spectrometry, using an assembly (reaction solution analysis) and disassembly (fragmentation of single crystals) approach. Overall, no significant differences between the Keggin POMs were found when changing the addenda metal atom (W or Mo) or the heteroatom (P or As); although small differences among the lowest-energy structures were detected.

Introduction

In recent years there has been an ever-increasing desire and drive for the design of molecules and their assembly into materials with programmed or designed functionality. Polyoxometalates (POMs) are a well-defined class of molecular metal-oxides formed from acid condensation of simple metal-oxides such as $W^{VI}O_4^{2-}$ and $Mo^{VI}O_4^{2-}$.[1] Consequently, the resulting metal-oxide clusters define an enormous class of accessible molecules with a wide addenda metal atom (*e.g.* W^{VI}, Mo^{VI}) nuclearity range from 6 to 368 metals in a single molecule.[2] Their unique structural and electronic properties, in particular their redox chemistry, are almost unmatched by any other general class of compound—an attribute that has seen them adopted in many areas: from catalysis and medicine, to material science and chemical analysis.[3] Thus uncovering the unique properties of POM architectures is one of the stepping stones towards technical innovation and tailoring their physicochemical properties in order to fully harness their power for application in catalysis and electronic materials.[4]

Since the most intense research focuses on the molecular and bulk properties of POMs,[5] a crucial gap remains in our understanding of the emergence of complexity in these molecular metal-oxide systems. Consequently, pathways towards the construction of nanoscale metal-oxide clusters (whose length scales vary from *ca.* 1–5 nm in size) are still unclear despite the vast number of well-defined geometries and nuclearities discovered to date (see Fig. 1). Interestingly, understanding the assembly of lower nuclearity POM systems will assist the synthesis of yet more complex high nuclearity species since the initial mechanisms of aggregation and formation are likely to be the same across the length scales.

Polyoxometalates are mostly synthesized by utilizing a 'one-pot' 'self-assembly' strategy which unsurprisingly hides a plethora of non-trivial assembly formation pathways which are inherently complex and ill-defined. Although considerable efforts have been made to accurately formulate and characterize the assembly processes behind the formation of POMs in general,[6] experimental and theoretical evidence to verify logical proposals are still relatively scarce. For several years now quantum

[a] *Departament de Química Física i Inorgànica, Universitat Rovira i Virgili, c/Marcel·lí Domingo s/n, 43007, Tarragona, Spain. E-mail: josepmaria.poblet@urv.cat; Web: http://www.quimica.urv.es/w3qf/; Fax: +34 977-559-563; Tel: +34 977-559-569*
[b] *WestCHEM, School of Chemistry, The University of Glasgow, Glasgow, UK G12 8QQ. E-mail: L.Cronin@chem.gla.ac.uk; Web: http://www.croninlab.com; Fax: +44 141-330-4888; Tel: +44 141-330-6650*

† Electronic supplementary information (ESI) available: Tables with the computed relative energies and figures for all the optimized structures analyzed in this work. Details on MS parameters and the data collection runs carried out as well as figures with representative fragmentation peaks. Details of the Experimental section. See DOI: 10.1039/c1cp21209e

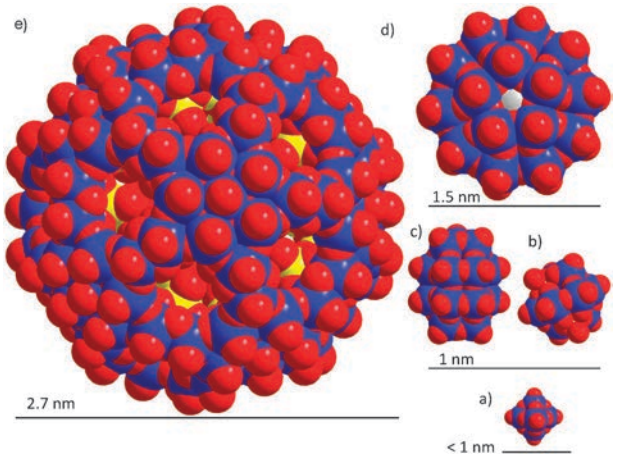

Fig. 1 Space filling models of nanoscale POM structures (to scale) illustrating the wide range of sizes that can be accessed (M: blue, O: red, S: yellow). (a) The $[M_6O_{19}]^{n-}$ Lindqvist anion; (b) the $[(XO_4)M_{12}O_{36}]^{n-}$ Keggin structure; (c) the $[(XO_4)_2M_{18}O_{54}]^{n-}$ Wells–Dawson polyanion made by the fusion of two Keggin fragments; (d) the $[NaP_5W_{30}O_{110}]^{14-}$ Preyssler anion; (e) $[Mo_{132}]$ Keplerate-type structure.

theory has been able to accurately describe the electronic structures of the polyoxoanions,[7] and complimentary analytical techniques such as single-crystal X-ray diffraction,[8] Mass Spectrometry[9] and NMR studies[10] can provide further evidence regarding nucleation mechanisms and structure–property correlations. We have previously reported a study where Mass Spectrometry and computational studies were combined to help reveal the initial cluster growth mechanisms of low-nuclearity POMs such as the Lindqvist anion, $[W_6O_{19}]^{2-}$.[11]

This study inspired us to suppose that it should be possible to build on the widely accepted bidentate addition mechanism proposed by Kepert in the 1960s, which is one of the only credible nucleation mechanisms previously proposed in polyoxometalate science.[12] Although in the 1970s, Tytko and Glemser expanded on these, providing more detailed mechanisms that dealt very well with the Kepert addition process.[13] In acidic media, protonation of $[MO_4]^{n-}$ leads to modification of the coordination geometry of the metal, for example $[MO_{6-y}(OH)_y]^{m-}$, and yields a polyoxometalate *via* a polycondensation reaction. The acidification of an aqueous solution of the $[MO_4]^{n-}$ starting material results in an expansion of the metal coordination shell from 4 to 6, *i.e.* from a tetrahedral (T_d) to an octahedral (O_h) oxygen coordination environment. This consequently enables protonation of the terminal oxygen atoms and facilitates condensation reactions between individual $[MO_6]$ fragments thereby resulting in the self-assembly of larger structures in solution. Typically, heteropolyanions result from the acidic polycondensation of $[MO_x]$ fragments around a central heteroelement, which behaves as a template to the forming structure meaning that the resulting symmetry and geometry depends strongly on the coordination geometry of the heteroanions. For example, under general POM reaction conditions, B tends to be trigonal; whereas Si, Ge, and P adopt a tetrahedral geometry; and transition metals such as Mo, W, Co and Ni prefer to be octahedral. Syntheses are complicated further still as the products are often dependent on the ratio of M : X in solution.

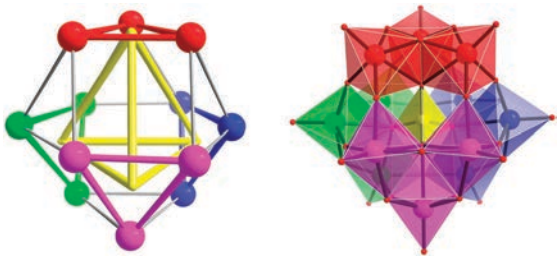

Fig. 2 Rationalization of the 12 metal-centered Keggin heteropolyoxoanion structure, $[\alpha\text{-}XM_{12}O_{40}]^{n-}$. The anion is composed of four independent $[M_3O_{13}]$ triads (red, green, magenta, blue) interconnected by threefold nodes only. The structure exhibits idealized tetrahedral (T_d) symmetry as indicated by the inscribed tetrahedron (yellow) which is introduced by the central templating anion $[XO_4]^{n-}$.

The formation of the 12 metal-centered Keggin anion, $[XM_{12}O_{40}]^{n-}$, can be considered to be a fundamental case of the self-assembly process involved in POM chemistry (see Fig. 2). This polyoxoanion structure is comprised of a tetrahedral template around which corner- and edge-sharing $[MO_6]$ octahedra bind. As such, the Keggin heteropolyanion can be dissected into distinctive principal building units: four trinuclear $[M_3O_{13}]$ triads—which are assembled from three edge-sharing $[MO_6]$ octahedra—arranged around a central $[XO_4]$ heteroanion template so that the central μ_3-oxygen ligand of each $[M_3O_{13}]$ fragment links to the central heteroatom X (where X = P, As, S *etc.*) (Fig. 2). The resultant cluster anion is a dodecanuclear metal-oxide anion with tetrahedral symmetry where each metal centre occupies the corner of a truncated tetrahedron. Baker and Figgis[14] postulated the existence of five isomers for the metal-oxide core of the Keggin anion, $[XM_{12}O_{40}]^{n-}$ arising from the rotation of $[M_3O_{13}]$ triads. The corresponding energy scale is commensurate with the experimental findings showing that as the number of rotated triads increases, so too does the energy of the metal-oxide core, resulting in the order $\alpha < \beta < \gamma < \delta < \varepsilon$. In addition, the molecular formula remains the same in all cases; but the redox properties do not. A combination of experimental[15,16] and theoretical[17,18] data proves that the redox properties vary from isomer to isomer;[19] however, fully oxidized Keggin anions prefer to adopt the α arrangement,[20] a result which has been further verified by theoretical evidence.[21]

Herein we expand on our previous observations concerning the nucleation mechanisms of small polyoxoanions and provide insight into the first steps of formation of larger 12-metal-centered Keggin heteropolyoxometalates, $[XM_yO_z]^{q-}$. This unique combination of experiment and theory serves as a powerful tool for rationalizing the nucleation mechanisms of this class of compounds. Not only do we have a sound theoretical basis, but advances in high resolution electrospray mass spectrometry mean that we are able to observe large and complex polyoxometalate clusters and fragments that were transmitted from the solution phase.[22]

Results and discussion

To develop our understanding of the nucleation processes involved in Keggin formation, Density Functional Theory (DFT) was used to model the energetics of the possible

nucleation steps towards the formation of this type of POM. To support this theoretical study, a series of Keggin-type polyoxometalate anions were synthesized and transferred to the gas phase *via* electrospray ionization (ESI), and the fragmentation products of these anions examined by collision-induced dissociation (CID). Fragmentation provides insight into the favored decomposition pathways of gas-phase clusters and, in combination with ESI-MS studies of their assembly, provides broader understanding of the intermediates relevant to their formation.

First steps in the formation of the Keggin anion

The formation of heteropolyoxoanions from the hydrogen-metalate anion, $[MO_3(OH)]^-$ (M = W, Mo), and the hetero-anion, $[XO_2(OH)_2]^-$ (X = P, As), which are abundant species under the conditions for synthesis of POMs, requires several steps of protonation and water condensation. In particular, up to 10 protonations and 12 water condensations are stoichiometrically required to obtain the Keggin anion, $[XM_{12}O_{40}]^{n-}$. We recently proposed formation mechanisms for the Lindqvist anion[11a] and we also postulate here that once the dinuclear species are formed, consecutive steps of protonation and water condensation followed by aggregation occur consistent with the clusters observed in the ESI-MS experiments. Two different dinuclear species are now viable: either the isodimer, $[M_2O_6(OH)_2]^{2-}$, occurring in the first formation step of the Lindqvist anion; or the heterodimer, $[MXO_5(OH)_3]^{2-}$. Standard DFT studies at the BP86/TZP level taking into account the effect of the solvent in a continuous manner (COSMO methodology),[23a] along with the results obtained from the ESI-MS experiments, point to the formation of the iso- instead of the heterodimer. Formation of the isodimer is energetically more feasible than the formation of the heterodimer according to the reaction energies (see Table 1) and to the estimated reaction free energies (see ESI†). The first step, the simple aggregation of two monomeric building blocks, is much more favoured for the iso-, $[M_2O_6(OH)_2]^{2-}$, than for the heterodimer, $[MXO_5(OH)_3]^{2-}$, regardless of the metal M and the hetero-atom X. The reaction for the ditungstate is moderately exothermic (-7.4 kcal mol^{-1}) whereas for the dimolybdate it is slightly endothermic ($+0.4$ kcal mol^{-1}). They are both, however, more exothermic (less endothermic) than those for the heterodimers, especially when the metal is tungsten (more than 8 kcal mol^{-1}). The second step, corresponding to water condensation preceded (2b′) or not (2a′ in Table 1) by protonation, is somewhat more favored for the heterodimers. This notwithstanding, the formation of the dehydrated isodimers is still more favored than those of the heterodimers in most of the cases. The reaction energy with respect to the monomers for the formation of the $[W_2O_7]^{2-}$ ditungstate is more exothermic than those for the phospho and the arsenotungstate (-5.3 *vs.* $+0.8$ and -0.3 kcal mol^{-1}, respectively, see Table 1). The differences are smaller for the case of molybdates, the isodimer being still slightly favored with respect to the formation of the phospho and arsenomolybdate (-2.3 *vs.* $+1.5$ and $+0.1$ kcal mol^{-1}). The formation of the $[M_2O_6(OH)]^-$ isodimers are favored with respect to the phosphometalates (-21.8 *vs.* -18.6 kcal mol^{-1} for M = W; and -17.9 *vs.* -17.2 kcal mol^{-1} for M = Mo), but the arsenometalates are competitive with the isodimers (see Table 1), especially in the case of molybdates. Therefore, in most of the cases analyzed here the heteroanion is predicted to be incorporated in later steps of the aggregation process. Analogous results are obtained when estimated reaction free energies are considered (see ESI†). The lowest-energy structures for $[XMO_5(OH)_3]^{2-}$, $[XMO_6(OH)]^{2-}$ and $[XMO_5(OH)_2]^-$ stoichiometries (steps 1′, 2a′ and 2b′ in Table 1, respectively) are depicted in Fig. 3.

Other structures together with their relative energies are shown in the ESI† (Fig. S1 and Table S1). For all of them, the M atom is five-coordinated and the X atom is four-coordinated (what we call 5c–4c structures). 5c–5c structures show much higher energies, especially for the case in which X = P, due to the preference of the heteroatom to remain with a tetrahedral environment (see Table S1 and Fig. S1, ESI†).

We have also analyzed the formation of these heterodimers by means of Car–Parrinello molecular dynamics simulations in combination with the metadynamics approach, which is used to accelerate the dynamics and to compute free-energy barriers.[23b–d] This methodology has been shown to be valid in previous studies as for example the formation mechanisms of the Lindqvist anion $[W_6O_{19}]^{2-}$.[11,24] The studied system was formed by one $[WO_3(OH)]^-$ monomer, one $[PO_2(OH)_2]^-$ heteroanion and 27 H_2O molecules. To describe the formation of heterodinuclear species in solution we used as a single collective variable (CV) the coordination number of the W atom with respect to the eight O atoms that belong to the WO_4 and PO_4 groups, C_{W-O}. The evolution of the coordination number C_{W-O} along the 20-ps metadynamics trajectory is shown in Fig. 4. A qualitative description of the events observed in this metadynamics follows. We observe the formation of the $[XMO_5(OH)_3]^{2-}$ heterodimer at the very beginning (0.2 ps) indicating that it is a likely event

Table 1 Energetics associated to the dimer formation[a,b]

Step		W–P	W–As	Mo–P	Mo–As	Process type
	Isodimer					
1	$\mathbf{[MO_3(OH)]^-_{(aq)}} + [MO_3(OH)]^-_{(aq)} \rightarrow \mathbf{[M_2O_6(OH)_2]^{2-}_{(aq)}}$	−7.4	−7.4	+0.4	+0.4	Aggregation
2a	$\mathbf{[M_2O_6(OH)_2]^{2-}_{(aq)}} \rightarrow \mathbf{[M_2O_7]^{2-}_{(aq)}} + H_2O_{(aq)}$	+2.1	+2.1	−2.7	−2.7	Water condensation
2b	$\mathbf{[M_2O_6(OH)_2]^{2-}_{(aq)}} + H_3O^+_{(aq)} \rightarrow \mathbf{[M_2O_6(OH)]^-_{(aq)}} + 2H_2O_{(aq)}$	−14.4	−14.4	−18.3	−18.3	Water condensation
	Heterodimer					
1′	$\mathbf{[MO_3(OH)]^-_{(aq)}} + [XO_2(OH)_2]^-_{(aq)} \rightarrow [XMO_5(OH)_3]^{2-}_{(aq)}$	+2.4	+1.3	+4.2	+3.7	Aggregation
2a′	$[XMO_5(OH)_3]^{2-}_{(aq)} \rightarrow [XMO_6(OH)]^{2-}_{(aq)} + H_2O_{(aq)}$	−1.6	−1.6	−2.7	−3.6	Water condensation
2b′	$[XMO_5(OH)_3]^{2-}_{(aq)} + H_3O^+_{(aq)} \rightarrow [XMO_5(OH)_2]^-_{(aq)} + 2H_2O_{(aq)}$	−21.0	−23.5	−21.4	−25.2	Water condensation

[a] Reaction energies are in kcal mol^{-1}. [b] The species detected in ESI-MS experiments are highlighted in bold.

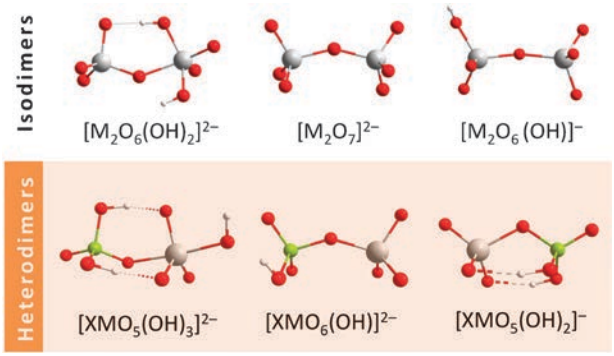

Fig. 3 Lowest-energy structures at the BP86/COSMO level for isodimers with $[M_2O_6(OH)_2]^{2-}$, $[M_2O_7]^{2-}$ and $[M_2O_6(OH)]^-$ stoichiometries (steps 1, 2a and 2b in Table 1, respectively) and for heterodimers with $[XMO_5(OH)_3]^{2-}$, $[XMO_6(OH)]^{2-}$ and $[XMO_5(OH)_2]^-$ stoichiometries (steps 1′, 2a′ and 2b′ in Table 1, respectively).

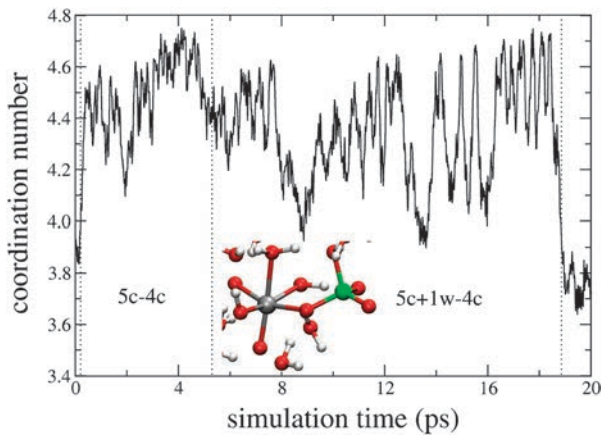

Fig. 4 Evolution of the coordination number C_{W-O} along the trajectory of the metadynamics run for the system formed by one $[WO_3(OH)]^-$ monomer, one $[PO_2(OH)_2]^-$ heteroanion and 27 H_2O molecules.

with a small barrier (around 1 kcal mol^{-1} according to our predictions).

At 3.6 ps, an intramolecular H^+ transfer from the O atom of the phosphate group to the O atom of the tungstate takes place making the W ion more electrophilic. As a consequence, at 5.2 ps a H_2O molecule is bonded to the W atom becoming now a six-coordinated ion. This **5c + 1w − 4c** structure (see Fig. 4, w stands for a coordinated water molecule) lasts for 13 ps and then the hydrated heterodimer is broken into the constituent monomers, *i.e.* the heteroanion and the hydrated $[WO_3(OH)]^-$ monomer. The stability of the hydrated heterodimer with respect to the monomers in terms of free energy is predicted to be around 15 kcal mol^{-1}. Additional metadynamics runs with the use of other collective variables (W···O distances, where the O atom belongs to the heteroanion, see Experimental section) were also performed and the same conclusions were retrieved.

Assembly and disassembly ESI-MS experiments

In order to investigate the initial steps of the assembly nucleation processes that yield the Keggin polyoxoanions $[XM_{12}O_{40}]^{3-}$ (X = P, As; M = W, Mo), established experimental procedures were followed to synthesize the series of Keggin anions,[25–27] and at the point where crystallization or precipitation was due to begin, the prepared solutions were transferred to the gas phase and analyzed by ESI-MS. It is noteworthy that a common feature of ESI is the observation of charge reduction during the electrospray process.[28] This has been attributed to the instability of highly charged clusters due to the Coulombic repulsion in the bare clusters following desolvation.[29] As a result, this charge reduction has two common manifestations: (i) ion association of discrete gas-phase ion clusters comprised of multiply charged polyoxoanions and multiple available counterions and (ii) protonation of oxo ligands of the cluster to form hydroxo ligands, often followed by a loss of water from the cluster framework. Importantly, the latter process results in the formal removal of O^{2-} from the polyoxoanion cluster.

For these assembly experiments, the assigned peaks corresponded to monomers and isodinuclear species, as for example: $[MO_3(OH)]^-$, $Na[MO_4]^-$, $Na[M_2O_7]^-$ and other species with different numbers of solvent molecules (water and acetonitrile, see Fig. S2 and S3, ESI† for more detailed description). In addition, for Mo-based Keggin anions, species such as $[Mo_2O_6(OH)]^-$ or $A[Mo_2O_6(OH)_2]^-$ (A: countercation), which were already postulated to be formed,[11] were also detected (see Fig. S4, ESI†). These experiments confirm the key theoretical predictions: that the heterodimers should form easily as a consequence of their small barrier of formation, but they are not observed because they are less stable than the isodinuclear species. Since the arsenometalates are predicted to be competitive with the isodimers, this appears as an apparent contradiction; however, the assembly experiments have been performed at *ca.* pH 5, so at these mildly acidic conditions formation of the isodimer (steps 1 and 2a, Table 1) might be favored with respect to formation of the heterodimer (steps 1′ and 2a′, Table 1). With the combined experimental and theoretical results obtained so far, we suggest that the isodimers are preferentially formed with respect to heterodimers in the conditions at which heteropolyanions are routinely synthesized.

At this point, the following question arose: would the heteroanion be incorporated in the next step of the reaction or would the isotrimer be formed? To address this query, fragmentation (disassembly) studies on solubilized single crystals of the same range of well-defined Keggin anions, transferred to the gas phase by ESI, were performed and provide us with important information relating to potential intermediates in their formation. Although collision induced dissociation (CID) very often may not access the same pathways as thermal assembly, due to both the absence of solvent and to the different energy ranges sampled, we have found this to be a useful tool in understanding the assembly of POM cluster anions;[11a] but especially useful in this current investigation when used in combination with the assembly studies mentioned previously.

In order to study the fragmentation of these anions, single crystal tetrabutylammonium salts ($[(n\text{-}C_4H_9)_4N]^+$ = TBA^+) were prepared. This cation exchange process was used primarily because TBA^+ cations have a much higher mass than Na^+ or K^+ and thus give a large separation between signals corresponding to differently-charged or protonated cluster

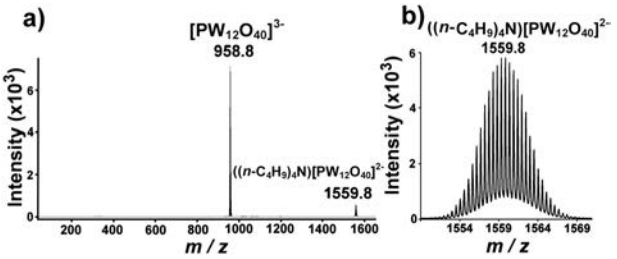

Fig. 5 Electrospray Ionisation Mass Spectrometry of $((n\text{-}C_4H_9)_4N)_3[PW_{12}O_{40}]$ showing (a) the major ions observed in the gas phase: $[XM_{12}O_{40}]^{3-}$ (*m*/*z* 958.8) and $((n\text{-}C_4H_9)_4N)[XM_{12}O_{40}]^{2-}$ (*m*/*z* 1559.8); and (b) the expanded *m*/*z* envelope at *m*/*z* 1559.8 which is assigned to the doubly charged anionic species $((n\text{-}C_4H_9)_4N)[XM_{12}O_{40}]^{2-}$.

states. Furthermore, the TBA^+ cations have a lower affinity for the POM cluster anions and solvent molecules than Na^+ or K^+ and consequently, the use of acetonitrile as a solvent prevents clusters from decomposing, aggregating, or converting into other species in solution or in the gas phase. Before disassembly, the major ions observed in the gas phase were $[XM_{12}O_{40}]^{3-}$ and $((n\text{-}C_4H_9)_4N)[XM_{12}O_{40}]^{2-}$ (see Fig. 5). Fragmentation of these species led to a range of anions in the gas phase (see Fig. S5 and S6, ESI†), the most intense of which being $[M_6O_{19}]^{2-}$. Upon increasing the collision energy the resulting collision induced dissociation (CID) of the parent Keggin anions produced low mass fragments assigned to $[M_xO_{3x+1}]^{2-}$ (x = 3–8), including heterotrimeric and tetrameric fragments such as $[PW_2O_9]^-$ and $[PW_2O_8(OH)_2]^-$ (see Fig. 6). Patterns of dissociation can be observed for all fragmented Keggin polyanions, for example the fragmentation of $((n\text{-}C_4H_9)_4N)_3[AsMo_{12}O_{40}]$ in acetonitrile produces key ions in the gas phase such as $((n\text{-}C_4H_9)_4N)[Mo_6O_{19}]^-$ (*m*/*z* 1122.0); $((n\text{-}C_4H_9)_4N)[Mo_7O_{22}]^-$ (*m*/*z* 1266.0) and $((n\text{-}C_4H_9)_4N)[Mo_8O_{25}]^-$ (*m*/*z* 1410.0). It is possible that these latter fragments in particular are the result of neutral losses of MoO_3 or Mo_2O_6 from parent ions, for example $((n\text{-}C_4H_9)_4N)[Mo_8O_{25}]^-$ to $((n\text{-}C_4H_9)_4N)[Mo_7O_{22}]^-$ and $((n\text{-}C_4H_9)_4N)[Mo_6O_{19}]^-$ (see Fig. S7, ESI†), although the trend in increasing collision energy indicated the progressive fragmentation of parent Keggin anions.

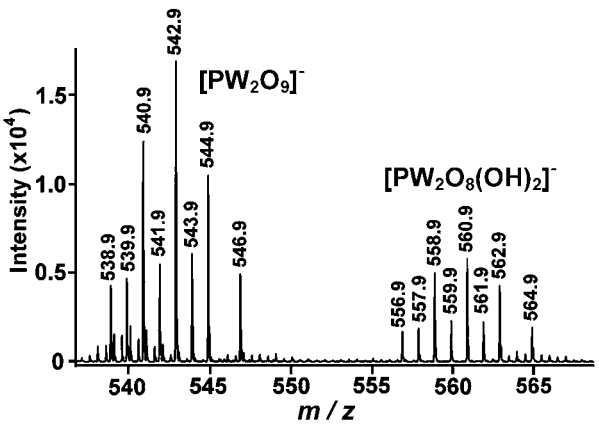

Fig. 6 Electrospray Ionisation Mass Spectrometry of single crystals of $((n\text{-}C_4H_9)_4N)_3[PW_{12}O_{40}]$ showing that, upon increasing the collision energy, the parent Keggin anions produce low mass heterotrimeric fragments such as $[PW_2O_9]^-$ (*m*/*z* 542.9) and $[PW_2O_8(OH)_2]^-$ (*m*/*z* 560.9).

Table 2 List of *m*/*z* peak assignments common to the assembly and fragmentation of all four Keggin polyoxoanions $[XM_{12}O_{40}]^{3-}$ (X = P, As; M = W, Mo)[a]

Common *m*/*z* peak assignments	
Assembly[a]	Fragmentation
$Na[MO_4]^-$	$[M_3O_{10}]^{2-}$
$[MO_3(OH)]^-$	$[M_4O_{13}]^{2-}$
$Na[M_2O_7]^-$	$[XM_3O_{12}]^-$
$[M_2O_6(OH)_2]^{2-}$	$[XM_4O_{15}]^-$
	$[M_5O_{16}]^{2-}$
	$[M_6O_{19}]^{2-}$
	$[M_7O_{22}]^{2-}$
	$[M_8O_{25}]^{2-}$
	$[XM_{12}O_{40}]^{3-}$
	$((n\text{-}C_4H_9)_4N)[XM_{12}O_{40}]^{2-}$
	$((n\text{-}C_4H_9)_4N)_2[XM_{12}O_{40}]^-$

[a] Refer to the Experimental section for reaction conditions followed.

Another example of such patterns comes from the fragmentation of $((n\text{-}C_4H_9)_4N)_3[PW_{12}O_{40}]$ in acetonitrile showing the presence of key doubly charged ions in the gas phase: $[W_3O_{10}]^{2-}$ (*m*/*z* 355.9); $[W_4O_{13}]^{2-}$ (*m*/*z* 471.9); $[W_5O_{16}]^{2-}$ (*m*/*z* 587.8) and $[W_6O_{19}]^{2-}$ (*m*/*z* 703.8) (see Fig. S8, ESI†). Table 2 (and expanded Table S2, ESI†) lists the *m*/*z* peak assignments common to all assembly and fragmentation ESI-MS experiments in this study, clearly showing the trend of the assembly up to isodimeric species and fragmentation down to isotrimeric species and heterotetrameric moieties.

Recently, Ma *et al.*[28] reported the gas phase fragmentation of selected classic phosphotungstate anions by multistage mass spectrometry experiments employing CID. The findings of this detailed study described how fragmentation of such polyoxoanions occurred *via* multiple reaction channels, resulting in pairs of complementary product anions whose total stoichiometry and charge matched those of the precursor anion. For example, $[PW_{12}O_{40}]^{3-}$ fragmented to give pairs of product ions of general formulas $[W_xO_{3x+1}]^{2-}$ and $[PW_{12-x}O_{39-3x}]^-$ (x = 6–9), and the most intense pair was found to be $[W_6O_{19}]^{2-}$ and $[PW_6O_{21}]^-$.

Next step: formation of heterotrinuclear species

Two tentative mechanisms are proposed for the formation of heterotrinuclear species according to the peak assignments in ESI-MS experiments of Keggin anions and based on the fact that protonation and water condensation steps are stoichiometrically necessary and the driving force in such nucleation processes (see Table 3). Stepwise protonations, with the subsequent condensation of water molecules, followed by aggregation of hydrogenmetalate anions seem a sensible proposal from the chemical point of view since the charge of the potential intermediates would not change significantly during the nucleation process. Other similar mechanistic proposals cannot, however, be discarded.

Reaction energies show that heterotrimers are more favoured than their iso- counterparts. Formation of $[XM_2O_9]^-$ from the isodimers (steps 3a–4a, Table 3) is more exothermic than formation of $[M_3O_{10}]^{2-}$: −12.6 (X = P) and −19.5 (X = As) *vs.* −1.7 kcal mol^{-1} for tungstates and −21.5 (X = P) and −25.5 (X = As) *vs.* −3.2 kcal mol^{-1} for molybdates. Similar results are obtained from the comparison between $[XM_2O_8(OH)_2]^-$ and $[M_3O_9(OH)]^-$ (steps 3b–4b, Table 3): −15.1 (X = P) and

Table 3 Energetics associated to the trimer formation[a,b]

Step		W–P	W–As	Mo–P	Mo–As	Process type
3a	$\mathbf{[M_2O_7]^{2-}_{(aq)}} + [XO_2(OH)_2]^-_{(aq)} \rightarrow [XM_2O_9(OH)_2]^{3-}_{(aq)}$	+1.3	+2.2	−0.5	−0.8	Aggregation
4a-1	$[XM_2O_9(OH)_2]^{3-}_{(aq)} + H_3O^+_{(aq)} \rightarrow [XM_2O_9(OH)]^{2-}_{(aq)} + 2H_2O_{(aq)}$	−18.4	−20.5	−20.1	−19.9	Water condensation
4a-2	$[XM_2O_9(OH)]^{2-}_{(aq)} + H_3O^+_{(aq)} \rightarrow \mathbf{[XM_2O_9]^-_{(aq)}} + 2H_2O_{(aq)}$	+4.5	−1.2	−0.9	−4.7	Water condensation
3b	$\mathbf{[M_2O_6(OH)]^-_{(aq)}} + [XO_2(OH)_2]^-_{(aq)} \rightarrow [XM_2O_8(OH)_3]^{2-}_{(aq)}$	−16.9	−6.6	−7.4	−5.4	Aggregation
4b	$[XM_2O_8(OH)_3]^{2-}_{(aq)} + H_3O^+_{(aq)} \rightarrow \mathbf{[XM_2O_8(OH)_2]^-_{(aq)}} + 2H_2O_{(aq)}$	+1.8	−7.0	−11.4	−10.9	Water condensation

[a] Reaction energies are in kcal mol^{-1}. [b] The species detected in ESI-MS experiments are highlighted in bold.

−13.6 (X = As) *vs.* −5.7 kcal mol^{-1} for tungstates and −18.8 (X = P) and −16.3 (X = As) *vs.* −8.4 kcal mol^{-1} for molybdates (see Fig. 7). Estimated reaction free-energies lead to the same conclusion (see ESI†).

The lowest-energy structures for $[XM_2O_9(OH)_2]^{3-}$, $[XM_2O_9(OH)]^{2-}$, $[XM_2O_9]^-$, $[XM_2O_8(OH)_3]^{2-}$, and $[XM_2O_8(OH)_2]^-$ stoichiometries are depicted in Fig. 8. We have analyzed a significant number of structures for each of these stoichiometries. The starting structures have been generated by chemical intuition and with the help of the metadynamics technique. All these structures along with their relative energies are shown in Fig. S10–S14 and Tables S3–S5 (ESI†). For $[XW_2O_9(OH)_2]^{3-}$ (step 3a), the lowest-energy structures feature a μ_3-O bridging atom (see Fig. 8a). None of the other structures show any μ_3-O bridging atom, *i.e.* they are not so compact, except one with a five-coordinated As atom which is 9.7 kcal mol^{-1} more unstable (Table S4, ESI†). The only structure in which the P atom is five-coordinated is very unstable compared to the other. For M = Mo, a similar structure with somewhat lower energy is found, but now with μ_2-O bridging atoms as a consequence of the lengthening of one of the Mo···O distances (see Fig. 8b). The compact structures with the μ_3-O atom are only 1 (X = P) and 3 kcal mol^{-1} (X = As) higher in energy. Open structures feature much higher energies. Similar conclusions are drawn for the structures with stoichiometry $[XM_2O_8(OH)_3]^{2-}$ (step 3b), which only differs in an extra H^+ from the stoichiometry previously analyzed. Now, the lowest-energy structure is that with the μ_3-O atom for both M = W and Mo (see Fig. 8h). For $[XM_2O_9(OH)]^{2-}$ (step 4a-1), the most stable structure for all the four possible

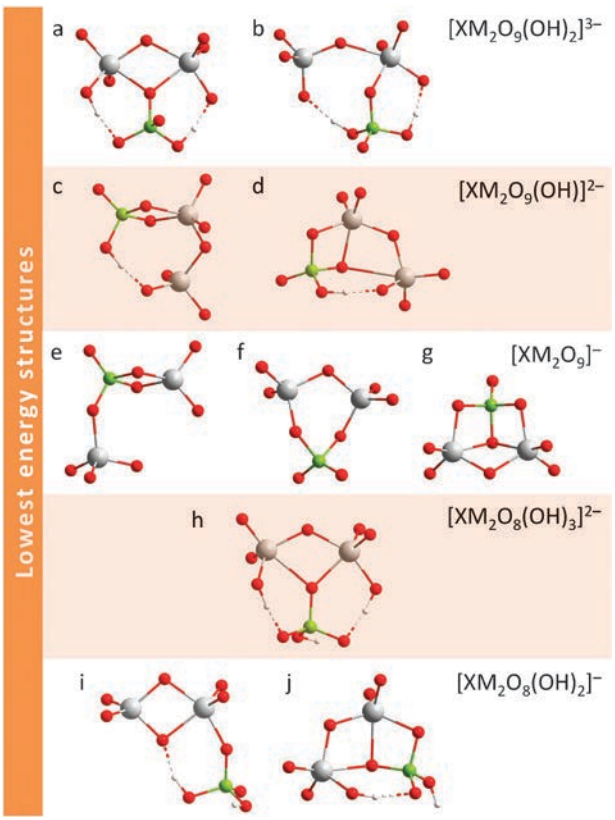

Fig. 8 Lowest-energy structures at the BP86/COSMO level for heterotrimers with $[XM_2O_9(OH)_2]^{3-}$, $[XM_2O_9(OH)]^{2-}$, $[XM_2O_9]^-$, $[XM_2O_8(OH)_3]^{2-}$, and $[XM_2O_8(OH)_2]^-$ stoichiometries.

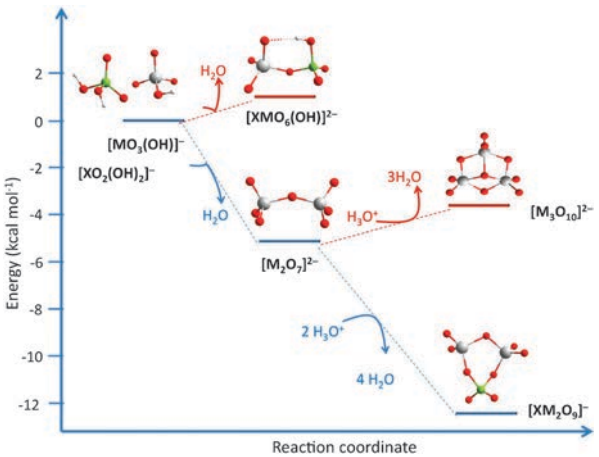

Fig. 7 Energetic profile associated to the formation of the dinuclear and trinuclear clusters, depicted energy values correspond to M = W and X = P.

species (M = W, Mo and X = P, As) shows the heteroanion coordinated to the metal in a bidentate fashion, but without the presence of any μ_3-O atom (see Fig. 8c). A structure in which the heteroanion also acts as a bidentate ligand but with a μ_3-O atom is only about 1 (M = Mo) and 3 kcal mol^{-1} (M = W) higher in energy (Fig. 8d). For $[XM_2O_8(OH)_2]^-$ (step 4b), with an extra H^+ with respect to the previous stoichiometry, the lowest-energy structure for all the species, except for M = W and X = As, shows now the heteroanion coordinated to the metal in a monodentate fashion without any μ_3-O atom (Fig. 8i). For $[AsW_2O_8(OH)_2]^-$ a most compact structure with a μ_3-O atom is predicted to be the most stable one (Fig. 8j). Finally, for $[XM_2O_9]^-$ (step 4a-2), compact and closed structures are by far much more stable than open and linear ones. The most stable structures show the heteroanion acting as a tri- or bidentate ligand yielding fairly compact structures which can be open or closed as a ring (Fig. 8e and f, respectively). A structure with a

μ_3-O atom and the heteroanion acting as a tridentate ligand shows somewhat higher energies, which range between 3 and 6 kcal mol^{-1} depending on the species in consideration (Fig. 8g).

It is important to remark at this point that most of the lowest-energy structures found for each stoichiometry, discussed above and shown in Fig. 8, are within a range of few kcal mol^{-1}. So, their relative stabilities might vary somewhat with changes in the computational settings, as for example the density functional or the solvation model. Moreover, neither explicit solvent molecules nor countercations are considered within the standard BP86/COSMO methodology. As a consequence, we can only safely state that some structures are favored with respect to others when their relative energies are significantly large, as for example comparing open and compact structures.

Car–Parrinello simulations, in combination with the metadynamics approach, have been also performed to analyze the formation of the heterotrimers. The system was built up by one $[W_2O_6(OH)]^-$ dimer, one $[PO_2(OH)_2]^-$ heteroanion and 58 H_2O molecules. The coordination number of the W ions with respect to the O atoms of the phosphate was selected as a collective variable (see Experimental section for details). Standard Car–Parrinello simulations previous to the metadynamics already show that the heterotrimer is formed when the nucleophilic O atom of the $[PO_2(OH)_2]^-$ heteroanion attacks one of the W^{VI} ions of the $[W_2O_6(OH)]^-$ dimer. As a consequence, the barrier for this process will be small. Hydration of the dimer was previously observed as well. So, the W^{VI} ions want to expand their coordination sphere so as to get to a pseudo-octahedral environment.

The coordination of the OH group of the heteroanion to the electrophilic W^{VI} ion of the dihydrated $[W_2O_6(OH)]^-$ dimer is not so effective (*i.e.* fast) as that of the oxo group in good agreement with its lower nucleophilicity. The estimation of the free-energy barrier for this process is 13 kcal mol^{-1}. Several common events are observed in these simulations: (i) the P atom remains as four-coordinated during the whole trajectory; (ii) the W^{VI} ions are hydrated becoming six-coordinated; and (iii) intramolecular H-bonds and proton transfers are effective involving the coordinated H_2O molecules and the oxo and hydroxo groups of the tungstate and the heteroanion (see Fig. 9 for a long-lived structure in the simulations).

From a metadynamics run on the system built up from one $[W_2O_6(OH)]^-$ dimer, one $[WO_3(OH)]^-$ monomer and 58 H_2O molecules we have also analyzed the formation and stability of the isotrimer (see Experimental section for details).

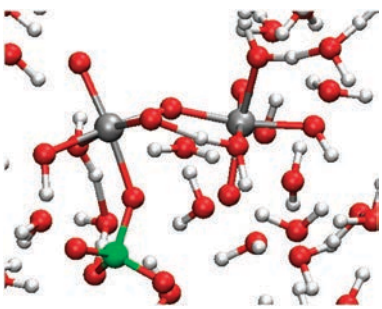

Fig. 9 Heterotrinuclear species from one metadynamics run for the system formed by $[W_2O_6(OH)]^-$ dimer, one $[PO_2(OH)_2]^-$ heteroanion and 58 H_2O molecules.

We predict an almost negligible formation barrier and stability comparable to the heterotrimer, albeit somewhat lower, but in good agreement with experiments.

Tetranuclear species and higher stages of aggregation

Once the heterotrimers are formed, aggregation of a new $[WO_3(OH)]^-$ monomer is postulated (see Table 4). In this case, the resulting species, $[XM_3O_{12}(OH)]^{2-}$ and $[XM_3O_{11}(OH)_3]^{2-}$, would lead to the stoichiometries $[XM_3O_{12}]^-$ and $[XM_3O_{11}(OH)_2]^-$, respectively, after just one protonation step and water condensation, which are also observed in the ESI-MS experiments. Thus far we have only analyzed the addenda metal W. As for lower nuclearity stages, we have performed an exhaustive study considering a large number of structures for each of these stoichiometries. All these structures along with their relative energies are shown in Fig. S15–S18 and Tables S6–S9 (ESI†). For $[XW_3O_{12}(OH)]^{2-}$ (step 5a, Table 4), the lowest-energy structure shows a μ_3-O bridging atom within a planar W_3 motif (Fig. 10a), which has been shown to be very stable.[11] This structure, in which the heteroanion is acting as a bidentate ligand, is by far the most stable among those that we have computed (more than 10 kcal mol^{-1} for X = P). Different positions and orientations of the H atom on the two terminal O atoms of the heteroanion lead to almost-degenerate structures (see Fig. S17 and Table S8 in the ESI†). For $[XW_3O_{12}]^-$ (step 6a), the lowest-energy structure presents a μ_4-O bridging atom with the heteroanion acting as a tridentate ligand (Fig. 10b). Another closed cyclic structure that is less compact (Fig. 10c) shows somewhat higher energies (around 5 kcal mol^{-1} for both X = P and As). Other, more tensioned compact structures are at least 10 kcal mol^{-1} higher in energy. The linear structures are even more unstable (see Table S9 and Fig. S18, ESI†).

Regarding $[XW_3O_{11}(OH)_3]^{2-}$ (step 5b, Table 4), the lowest-energy structure for both X = P and As also shows a μ_3-O bridging atom within a planar W_3 motif (see Fig. 10d). In this case the heteroanion is acting as a monodentate ligand forming hydrogen bonds with the W_3 motif. This structure is by far the most stable among all those that we have computed (around 13 and 20 kcal mol^{-1} for X = P and As, respectively). Finally, for $[XW_3O_{11}(OH)_2]^-$ (step 6b) the two most-stable structures are also depicted in Fig. 10e and f. These two structures show an energy difference of around 4 kcal mol^{-1} for X = P, but they are quasidegenerate for X = As. In both of them, the heteroanion is acting as a bidentate ligand. The most important difference is that the most stable structure presents a μ_3-O bridging atom involving the heteroanion (Fig. 10e). Other symmetric and compact structures are found within less than 10 kcal mol^{-1} compared to the most-stable one (see structure 4 in Fig. S16, ESI†). As a general trend, the heteroatom is tetracoordinated in all the structures with the lowest energies among the different stoichiometries that we have analyzed here.

Aggregation of another $[MO_3(OH)]^-$ monomer to the $[XM_3O_{12}]^-$ species, followed by protonation and dehydration, justifies the ESI peak corresponding to $[XM_4O_{15}]^-$. Similar steps would follow to finally lead, after a total of 10 protonations and 12 dehydrations, to the Keggin anion. Peaks corresponding to higher nuclearities in the $[XM_xO_{3x+3}]^-$ series (x = 5 and 6) have

Table 4 Energetics associated to the tetramer formation[a,b]

Step		W–P	W–As	Process type
5a	$\mathbf{[XM_2O_9]^-_{(aq)}} + [MO_3(OH)]^-_{(aq)} \rightarrow [XM_3O_{12}(OH)]^{2-}_{(aq)}$	−31.6	−25.1	Aggregation
6a	$[XM_3O_{12}(OH)]^{2-}_{(aq)} + H_3O^+_{(aq)} \rightarrow \mathbf{[XM_3O_{12}]^-_{(aq)}} + 2H_2O_{(aq)}$	+1.0	−2.8	Water condensation
5b	$\mathbf{[XM_2O_8(OH)_2]^-_{(aq)}} + [MO_3(OH)]^-_{(aq)} \rightarrow [XM_3O_{11}(OH)_3]^{2-}_{(aq)}$	−20.2	−18.4	Aggregation
6b	$[XM_3O_{11}(OH)_3]^{2-}_{(aq)} + H_3O^+_{(aq)} \rightarrow \mathbf{[XM_3O_{11}(OH)_2]^-_{(aq)}} + 2H_2O_{(aq)}$	+6.7	+10.2	Water condensation

[a] Reaction energies are in kcal mol^{-1}. [b] The species detected in ESI-MS experiments are highlighted in bold.

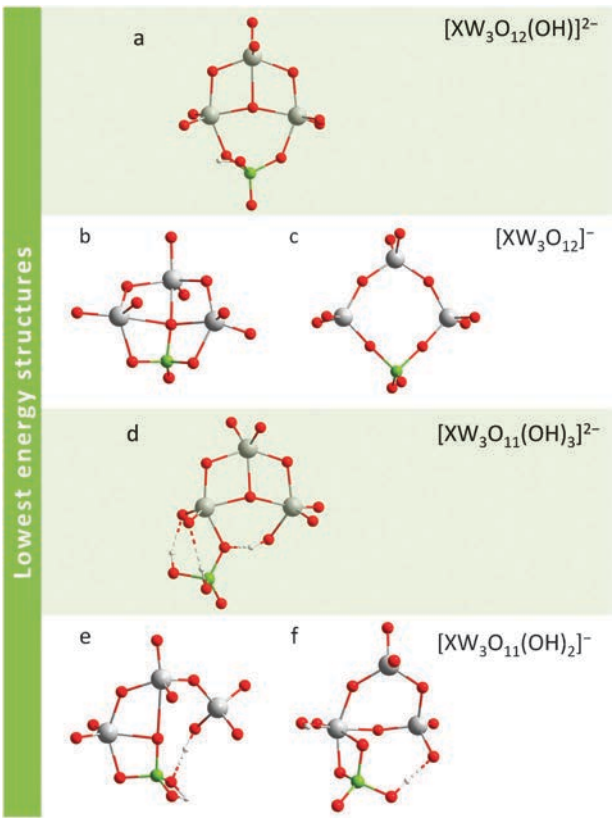

Fig. 10 Lowest-energy structures at the BP86/COSMO level for heterotetramers with $[XW_3O_{12}(OH)]^{2-}$, $[XW_3O_{12}]^-$, $[XW_3O_{11}(OH)_3]^{2-}$, and $[XW_3O_{11}(OH)_2]^-$ stoichiometries.

been detected in previous ESI-MS experiments.[25] These species, not observed here, may have been fragmented using our experimental settings and were subsequently not detected. To conclude, we would like to point out that the heteropolynuclear species formed in the early steps of the nucleation process, which we have analyzed in detail here, might develop not only to the Keggin anion, but also to other heteroPOMs such as the Wells–Dawson, $[P_2W_{18}O_{62}]^{6-}$, or the Preyssler, $[NaP_5W_{30}O_{110}]^{14-}$, anions depending on the particular experimental reaction conditions, *i.e.* temperature, solvent, pH, counterions, *etc.* Interestingly, the peak corresponding to $[XM_3O_{12}]^-$ has been detected in ESI-MS experiments on the Wells–Dawson anion as well as in some of its lacunary derivatives.[25]

Conclusions

In this article we have reported our studies on the first steps of nucleation responsible for the formation of Keggin heteropolyanions using the complimentary combination of DFT methodologies and ESI-MS. As previously described for the Lindqvist isopolyanion,[11a] we postulate that once the dinuclear $[M_2O_7]^{2-}$ species have been formed, successive steps of protonation and water condensation with subsequent aggregation occur forming the Keggin heteropolyanions. This tentative mechanistic proposal is based not only on chemical intuition, but also on computational results and the cluster species observed in the ESI-MS experiments. We propose that the heteroanion, $[XO_2(OH)_2]^-$, is not incorporated into the polyanion initially, in the first steps of the nucleation, *i.e.* forming a heterodimer; but in a later step. Thereafter formation of the heterotrimer, the heteroanion, $[XO_2(OH)_2]^-$, acts as a template for the formation of the Keggin anion. The structure and stability of different possible intermediates in the first steps of the formation of the Keggin anion according to our proposed mechanisms have been analyzed in detail using Density Functional Theory. In general, no significant differences were found when changing the metal atom (W or Mo) or the heteroatom (P or As), except that arsenometalate heterodimers might be competitive with isodimers at low pH conditions. Thermal and entropic effects, yet non-negligible for some of the reactions, do not alter the abovementioned main conclusions obtained from reaction energies based on the potential energy surfaces. We have complemented our theoretical studies by using assembly–disassembly experiments using Electrospray Ionization Mass Spectrometry. By solubilizing single crystals of plenary Keggin heteropolyanions and transferring into the gas phase using ESI we have been able to study fragmentation (disassembly) profiles of parent heteropolyanions; while analysis of the reaction solutions *via* the same ESI-MS methods provided detailed information on the assembly processes involved. Although CID very often may not access the same pathways as thermal assembly, due to both the absence of solvent and to the different energy ranges sampled, it might provide hints to help in understanding the assembly of polyoxoanions. In summary, the present study on the nucleation mechanisms of heteropolyanions, which complements the previous work on the Lindqvist isopolyanion, provides crucial new information towards the rationalization of the complex processes that take place in the formation of heteropolyanions, an understanding that facilitates the design of yet more complex and higher nuclearity POMs.

Experimental section

Fragmentation experiments

For the ESI-MS fragmentation experiments, $Na_2HPMo_{12}O_{40}\cdot 14H_2O$, $Na_3PW_{12}O_{40}\cdot 12H_2O$, $((n\text{-}C_4H_9)_4N)_3[AsMo_{12}O_{40}]$, and $Na_3AsW_{12}O_{40}\cdot xH_2O$ were synthesized using the reported procedures of Rocchiccioli-Deltcheff *et al.*,[25] North,[26]

Sanchez *et al.*[27] and Rocchiccioli-Deltcheff *et al.*,[25] respectively. Tetra-*n*-butylammonium salts (TBA = $[(n\text{-}C_4H_9)_4N]$) of these Keggin anions were also prepared (see ESI†). Their identities were confirmed by single-crystal X-ray diffraction and elemental analysis (see ESI†). The MS samples were prepared by dissolution of 10 mg of TBA-Keggin salt in 5 mL CH_3CN and sonicated for 15 min; 20 μL of this solution was made up to 4 mL with CH_3CN. All MS data were collected using a Q-trap, time-of-flight MS (MicroTOF-Q MS) instrument equipped with and electrospray ionisation (ESI) source supplied by Bruker Daltonics Ltd. The detector was a micro-channel plate detector, and all data were processed using the Bruker Daltonics Analysis 4.0 software; simulated isotope patterns were investigated using the Bruker Isotope Pattern software and Molecular Weight Calculator 6.45. See ESI† for more details on MS parameters and the data collection runs carried out.

Assembly experiments

$Na_2HPMo_{12}O_{40}\cdot 14H_2O$ was synthesized following the procedure described by Rocchiccioli-Deltcheff *et al.*[25] and the MS dilutions were prepared as follows: 0.450 mL (0.76 mmol) of H_3PO_4 85% was dissolved in 25 mL of aqueous 2.5 M $Na_2MoO_4\cdot 2H_2O$. Afterwards 1 mL of this mixture was diluted with 10 mL of H_2O and 10 mL of CH_3CN. Finally a small spatula tip (*ca.* 20 mg) of $(n\text{-}C_4H_9)_4NBr$ was dissolved into this solution. Aliquots of this final mixture were filtered to remove any particulates and analyzed by ESI-MS.

$Na_3PW_{12}O_{40}\cdot 12H_2O$ was synthesized following the procedure described by North[26] and the MS dilutions were prepared as follows: 0.450 mL (0.76 mmol) of H_3PO_4 85% was dissolved in 25 mL of aqueous 2.5 M $Na_2WO_4\cdot 2H_2O$. Afterwards 1 mL of this mixture was diluted with 10 mL of H_2O and 10 mL of CH_3CN. Finally a small spatula tip (*ca.* 20 mg) of $(n\text{-}C_4H_9)_4NBr$ was dissolved into this solution. Aliquots of this final mixture were filtered to remove any particulates and analyzed by ESI-MS.

$((n\text{-}C_4H_9)_4N)_3[AsMo_{12}O_{40}]$ was synthesized following the procedure described by Sanchez *et al.*[27] and the MS dilutions were prepared as follows: 7.2 g (0.049 mol) MoO_3, 0.63 g (2.73 mmol) As_2O_5 and 1.32 g (0.055 mol) LiOH were dissolved together in 20 mL of hot H_2O. Afterwards 1 mL of this mixture was diluted with 10 mL of H_2O and 10 mL of CH_3CN. Finally a small spatula tip (*ca.* 20 mg) of $(n\text{-}C_4H_9)_4NBr$ was dissolved into this solution. Aliquots of this final mixture were filtered to remove any particulates and analyzed by ESI-MS.

$Na_3AsW_{12}O_{40}\cdot xH_2O$ was synthesized following the procedure described by Rocchiccioli-Deltcheff *et al.*[25] and the MS dilutions were prepared as follows: 2 mL of 2 M sodium arsenate solution (prepared with 0.42 g of $3As_2O_5\cdot 5H_2O$ and 0.33 g of NaOH pellets) was poured into 10 mL of H_2O and 16.5 g (0.25 mol) $Na_2WO_4\cdot 2H_2O$ was added. Afterwards 1 mL of this mixture was diluted with 10 mL of H_2O and 10 mL of CH_3CN. Finally a small spatula tip (*ca.* 20 mg) of $(n\text{-}C_4H_9)_4NBr$ was dissolved into this solution. Aliquots of this final mixture were filtered to remove any particulates and analyzed by ESI-MS.

Computational methodology

The static calculations were carried out by using density functional theory (DFT) methodology with the ADF program.[30] The gradient-corrected functionals of Becke and Perdew for the exchange and correlation energies, respectively, were used to improve the description of the electronic density provided by the local density approximation (X-alpha functional for the exchange part and Vosko–Wilk–Nusair functional for the correlation part).[31] A set of Slater-type basis functions of triple-ξ + polarization quality was employed to describe the valence electrons of all the atoms. Scalar relativistic corrections were included by means of the zeroth-order regular approximation (ZORA) formalism. All the computed stationary points have a closed-shell electronic structure. All the structures discussed through this work were fully optimized in the presence of a continuous model solvent by means of the conductor-like screening model (COSMO) implemented in the ADF code (see ESI† for more details).[32] The dielectric constant (ε) is set to 78 so as to model water as a solvent. Calculations of harmonic frequencies confirm that all the lowest-energy structures for each of the stoichiometries computed in this work (structures in Fig. 3, 8 and 10) are minima of the potential energy surface. The higher-energy structures for which we have computed harmonic frequencies are also minima (for more details see the ESI†). Reaction free energies, based on the harmonic approximation, have been also estimated. Since the reaction takes place in a condensed phase, we have only taken into account the thermal and entropic vibrational contributions to the free energy (for more details see the ESI†).

Regarding the molecular dynamics (MD) simulations, they were performed at the DFT level by means of the CPMD program package.[33] The description of the electronic structure is based on the expansion of the valence electronic wave functions into a plane wave (PW) basis set, which is limited by an energy cutoff of 70 Ry. The interaction between the valence electrons and the ionic cores is treated through the pseudopotential (PP) approximation. Norm-conserving Martins–Troullier PPs are employed and nonlinear core corrections (NLCC) are included in the W PP.[34] We adopt the generalized gradient-corrected Becke–Lee–Yang–Parr (BLYP) exchange-correlation functional.[31a,35] The validity of these computational settings for the study of isopolyanions has been checked previously.[11,24a] In the MD simulations, the wave functions are propagated in the Car–Parrinello scheme, by integrating the equations of motion derived from the extended Car–Parrinello Lagrangian.[36] We use a time step of 0.144 fs and a fictitious electronic mass of 700 a.u. A simple rescaling of the atomic velocities keeps the temperature within an interval of 50 K around 300 K. The cell box that contains: (i) one $[WO_3(OH)]^-$, one $[PO_2(OH)_2]^-$ and 27 H_2O molecules ($a = b = c = 9.959$ Å) or (ii) one $[W_2O_6(OH)]^-$, one $[PO_2(OH)_2]^-$ and 58 H_2O molecules ($a = b = c = 12.580$ Å) is repeated periodically in space by the standard periodic boundary conditions. The limited simulation time affordable by standard MD runs does not allow the observation of rare events like thermally activated chemical reactions. For this reason, we use the metadynamics technique, which is capable of efficiently reconstructing complex reaction mechanisms and provides the free energy profile, as demonstrated in

previous applications.[24] A detailed description of the metadynamics method associated with Car–Parrinello MD can be found elsewhere (see ESI† for more details on the parameters used in the metadynamics runs).[23]

Acknowledgements

We acknowledge support from the MEC of Spain (project CTQ2008-06549-C02-01/BQU and the Ramón y Cajal Program (A.R.-F.)) and from the DGR of the Autonomous Government of Catalonia (grants 2009SGR462 and XRQTC). L.C. wishes to acknowledge the EPSRC, The University of Glasgow, WestCHEM, the Leverhulme Trust and the Royal Society/Wolfson Foundation for funding.

Notes and references

1 M. T. Pope, *Heteropoly and Isopoly Oxometalates*, Springer-Verlag, New York, 1983.
2 C. L. Hill, (Ed.), Special issue on polyoxometalates, *Chem. Rev.*, 1998, **98**, 1.
3 D. E. Katsoulis, A Survey of the Applications of Polyoxometalates, *Chem. Rev.*, 1998, **98**, 359.
4 D.-L. Long, R. Tsunashima and L. Cronin, *Angew. Chem., Int. Ed.*, 2010, **49**, 1736.
5 A. Müller and S. Roy, *Coord. Chem. Rev.*, 2003, **245**, 153.
6 D.-L. Long, E. Burkholder and L. Cronin, *Chem. Soc. Rev.*, 2007, **36**, 105.
7 (*a*) J. M. Poblet, X. Lopez and C. Bo, *Chem. Soc. Rev.*, 2003, **32**, 297; (*b*) H. Duclusaud and S. A. Borshch, *J. Am. Chem. Soc.*, 2001, **123**, 2825; (*c*) J. A. Fernandez, X. Lopez, C. Bo, C. de Graaf, E. J. Baerends and J. M. Poblet, *J. Am. Chem. Soc.*, 2007, **129**, 12244; (*d*) L. K. Yan, X. Lopez, J. J. Carbo, R. Sniatynsky, D. C. Duncan and J. M. Poblet, *J. Am. Chem. Soc.*, 2008, **130**, 8223.
8 (*a*) J. B. Strong, G. P. A. Yap, R. Ostrander, L. M. Liable-Sands, A. L. Rheingold, R. Thouvenot, P. Gouzerh and E. A. Maatta, *J. Am. Chem. Soc.*, 2000, **122**, 639; (*b*) R. Cao, K. P. O'Halloran, D. A. Hillesheim, K. I. Hardcastle and C. L. Hill, *CrystEngComm*, 2010, **12**, 1518.
9 (*a*) C. Dablemont, A. Proust, R. Thouvenot, C. Afonso, F. Fournier and J.-C. Tabet, *Inorg. Chem.*, 2004, **43**, 3514; (*b*) J. Yan, D.-L. Long, E. F. Wilson and L. Cronin, *Angew. Chem., Int. Ed.*, 2009, **48**, 4376.
10 (*a*) A. Bagno and M. Bonchio, *Angew. Chem., Int. Ed.*, 2005, **44**, 2023; (*b*) A. Bagno, M. Bonchio and J. Autschbach, *Chem.–Eur. J.*, 2006, **12**, 8460; (*c*) L. Vilà-Nadal, J. P. Sarasa, A. Rodríguez-Fortea, J. Igual, L. P. Kazansky and J. M. Poblet, *Chem.–Asian J.*, 2010, **5**, 97.
11 (*a*) L. Vilà-Nadal, A. Rodríguez-Fortea, L.-K. Yan, E. F. Wilson, L. Cronin and J. M. Poblet, *Angew. Chem., Int. Ed.*, 2009, **48**, 1; (*b*) L. Vilà-Nadal, A. Rodríguez-Fortea and J. M. Poblet, *Eur. J. Inorg. Chem.*, 2009, 5125.
12 D. L. Kepert, *Prog. Inorg. Chem.*, 1962, **4**, 199.
13 K. H. Tytko and O. Glemser, *Adv. Inorg. Chem. Radiochem.*, 1976, **29**, 239.
14 L. C. W. Baker and J. S. Figgis, *J. Am. Chem. Soc.*, 1970, **92**, 3794.
15 L. Lisnard, A. Dolbecq, P. Mialane, J. Marrot and F. Sécheresse, *Inorg. Chim. Acta*, 2004, **357**, 845.
16 T. McGlone, C. Streb, D.-L. Long and L. Cronin, *Chem.–Asian J.*, 2009, **4**, 1612.
17 H. N. Miras, J. Yan, D.-L. Long and L. Cronin, *Angew. Chem., Int. Ed.*, 2008, **47**, 8420.
18 M. T. Pope and A. Müller, *Angew. Chem., Int. Ed.*, 1991, **30**, 34.
19 (*a*) C. Baffert, J. F. Boas, A. M. Bond, P. Kögerler, D.-L. Long, J. R. Pilbrow and L. Cronin, *Chem.–Eur. J.*, 2006, **12**, 8472; (*b*) I.-M. Mbomekalle, X. López, J. M. Poblet, F. Sécheresse, B. Keita and L. Nadjo, *Inorg. Chem.*, 2010, **49**, 7001.
20 L. C. W. Baker, V. E. S. Baker, G. A. Candela, A. H. Kahan and S. H. Wasfi, *J. Chem. Phys.*, 1972, **56**, 4917.
21 X. López and J. M. Poblet, *Inorg. Chem.*, 2004, **43**, 6863.
22 (*a*) J. Yan, J. Gao, D.-L. Long, H. N. Miras and L. Cronin, *J. Am. Chem. Soc.*, 2010, **132**, 11410; (*b*) J. Yan, D.-L. Long, E. F. Wilson and L. Cronin, *Angew. Chem., Int. Ed.*, 2009, **48**, 4376; (*c*) H. N. Miras, E. F. Wilson and L. Cronin, *Chem. Commun.*, 2009, 1297; (*d*) Y.-F. Song, D.-L. Long, S. E. Kelly and L. Cronin, *Inorg. Chem.*, 2008, **47**, 9137; (*e*) E. F. Wilson, H. N. Miras, M. H. Rosnes and L. Cronin, *Angew. Chem., Int. Ed.*, 2011, **50**, 3720; (*f*) E. F. Wilson, H. Abbas, B. J. Duncombe, C. Streb, D.-L. Long and L. Cronin, *J. Am. Chem. Soc.*, 2008, **130**, 13876; (*g*) D.-L. Long, C. Streb, Y. F. Song, S. Mitchell and L. Cronin, *J. Am. Chem. Soc.*, 2008, **130**, 1830.
23 (*a*) X. López, J. A. Fernández, S. Romo, J. F. Paul, L. Kazansky and J. M. Poblet, *J. Comput. Chem.*, 2004, **12**, 1542; (*b*) M. Iannuzzi, A. Laio and M. Parrinello, *Phys. Rev. Lett.*, 2003, **90**, 238302; (*c*) A. Laio and M. Parrinello, *Proc. Natl. Acad. Sci. U. S. A.*, 2002, **99**, 12562; (*d*) A. Laio, A. Rodriguez-Fortea, F. L. Gervasio, M. Ceccarelli and M. Parrinello, *J. Phys. Chem. B*, 2005, **109**, 6714.
24 (*a*) A. Rodríguez-Fortea, L. Vilà-Nadal and J. M. Poblet, *Inorg. Chem.*, 2008, **47**, 7745; (*b*) X. Biarnes, A. Ardévol, A. Planas, C. Rovira, A. Laio and M. Parrinello, *J. Am. Chem. Soc.*, 2007, **129**, 10686; (*c*) J. Blumberger, B. Ensing and M. L. Klein, *Angew. Chem., Int. Ed.*, 2006, **45**, 2893; (*d*) A. Rodríguez-Fortea and M. Iannuzzi, *J. Phys. Chem. C*, 2008, **112**, 19642; (*e*) A. Rodríguez-Fortea, M. Iannuzzi and M. Parrinello, *J. Phys. Chem. C*, 2007, **111**, 2251; (*f*) A. Rodríguez-Fortea, M. Iannuzzi and M. Parrinello, *J. Phys. Chem. B*, 2006, **110**, 3477; (*g*) A. Stirling, M. Iannuzzi, M. Parrinello, F. Molnar, V. Bernhart and G. A. Luinstra, *Organometallics*, 2005, **24**, 2533.
25 C. Rocchiccioli-Deltcheff, M. Fournier, R. Franck and R. Thouvenot, *Inorg. Chem.*, 1983, **22**, 207.
26 E. O. North, *Inorg. Synth.*, 1939, **1**, 132.
27 C. Sanchez, J. Livage, J. P. Launay, M. Fournier and Y. Jeanin, *J. Am. Chem. Soc.*, 1982, **104**, 3194.
28 (*a*) M. T. Ma, T. Waters, K. Beyer, R. Palamarczuk, P. J. Richardt, R. A. J. O'Hair and A. G. Wedd, *Inorg. Chem.*, 2009, **48**, 598; (*b*) C. Boglio, G. Lenoble, C. Duhayon, B. Hasenknopf, R. Thouvenot, C. Zhang, R. C. Howell, B. P. Burton-Pye, L. C. Francesconi, E. Lacôte, S. Thorimbert, M. Malacria, C. Afonso and J.-C. Tabet, *Inorg. Chem.*, 2006, **45**, 1389.
29 (*a*) T. Waters, X. Huang, X.-B. Wang, H.-K. Woo, R. A. J. O'Hair, A. G. Wedd and L.-S. Wang, *J. Phys. Chem. A*, 2006, **110**, 10737; (*b*) H.-J. Zhai, X. Huang, T. Waters, X.-B. Wang, R. A. J. O'Hair, A. G. Wedd and L.-S. Wang, *J. Phys. Chem. A*, 2005, **109**, 10512; (*c*) L.-S. Wang and X.-B. Wang, *J. Phys. Chem. A*, 2000, **104**, 1978.
30 (*a*) ADF 2004.01, Department of Theoretical Chemistry, Vrije Universiteit, Amsterdam; (*b*) G. T. te Velde, F. M. Bickelhaupt, E. J. Baerends, C. F. Guerra, S. J. A. Van Gisbergen, J. G. Snijders and T. Ziegler, *J. Comput. Chem.*, 2001, **22**, 931.
31 (*a*) A. D. Becke, *Phys. Rev. A*, 1988, **38**, 3098; (*b*) J. P. Perdew, *Phys. Rev. B: Condens. Matter*, 1986, **33**, 8822; (*c*) S. H. Vosko, L. Wilk and M. Nusair, *Can. J. Phys.*, 1980, **58**, 1200.
32 (*a*) A. Klamt and G. J. Schuurmann, *J. Chem. Soc., Perkin Trans. 2*, 1993, 799; (*b*) A. Klamt, *J. Phys. Chem.*, 1995, **99**, 2224; (*c*) C. C. Pye and T. Ziegler, *Theor. Chem. Acc.*, 1999, **101**, 396.
33 CPMD, IBM Corp., Armonk, NY, 1990–2006; MPI für Festkörperforschung, Stuttgart 1997–2001.
34 (*a*) N. Troullier and J. L. Martins, *Phys. Rev. B: Condens. Matter*, 1991, **43**, 1993; (*b*) S. G. Louie, S. Froyen and M. L. Cohen, *Phys. Rev. B: Condens. Matter*, 1982, **26**, 1738.
35 C. Lee, W. Yang and R. Parr, *Phys. Rev. B: Condens. Matter*, 1988, **37**, 785.
36 R. Car and M. Parrinello, *Phys. Rev. Lett.*, 1985, **55**, 2471.